catalysts

MDPI

Article

Application of Composite Film Containing Polyoxometalate Ni25 and Reduced Graphene Oxide for Photoelectrocatalytic Water Oxidation

Jianye Pei and Lihua Bi *

College of Chemistry, Jilin University, Changchun 130021, China; peijy20@mails.jlu.edu.cn
* Correspondence: blh@jlu.edu.cn

Abstract: The preparation of clean energy is an effective way to solve the global energy crisis and reduce environmental pollution. The decomposition of water can produce hydrogen and oxygen, which is one of the effective ways to prepare clean energy. However, water oxidation is a bottleneck for water decomposition, thus, developing a water oxidation catalyst can accelerate the process of water decomposition to generate clean energy. Nickel-substituted polyoxometalate $[Ni_{25}(H_2O)_2(OH)_{18}(CO_3)_2(PO_4)_6(SiW_9O_{34})_6]^{50-}$ (Ni25) is proven as an excellent water oxidation photocatalyst. To develop the effective photoelectrocatalyst for water oxidation, in this work, we constructed two composite films containing Ni25 on ITO, $[PDDA/Ni25]_n$, and $PDDA/[Ni25/(PDDA–rGO)]_n$, by layer-by-layer self-assembly, which is the first combination of nickel-substituted polyoxometalates and reduced graphene oxide (rGO). The study on the photoelectrocatalytic performance of the two films indicates that the water oxidation current of the film $PDDA/[Ni25/(PDDA–rGO)]_n$-modified electrode is increased by 33.7% after light irradiation, which is 1.71 times that of the film $[PDDA/Ni25]_n$-modified electrode. Moreover, the transient photocurrent response of the film $PDDA/[Ni25/(PDDA–rGO)]_n$-modified electrode demonstrates that there is a synergistic effect between rGO and Ni25, and rGO-accelerated electron transport and inhibited charge recombination. In addition, the film $PDDA/[Ni25/(PDDA–rGO)]_n$-modified electrode exhibits good stability, indicating its great potential as an effective photoelectrocatalyst for water oxidation in practical application.

Keywords: polyoxometalate; nickel; reduced graphene oxide; photoelectrocatalysis; water oxidation

Citation: Pei, J.; Bi, L. Application of Composite Film Containing Polyoxometalate Ni25 and Reduced Graphene Oxide for Photoelectrocatalytic Water Oxidation. *Catalysts* **2022**, *12*, 696. https://doi.org/10.3390/catal12070696

Academic Editor: Lucian Baia

Received: 11 April 2022
Accepted: 22 June 2022
Published: 24 June 2022

1. Introduction

In order to meet the large amount of energy required for human beings' daily activities, the continuous use of fossil fuel has led to excessive emissions of carbon dioxide and other greenhouse gases. This led to consequences such as global warming, rising sea levels, and the energy crisis; thus, exploring clean energy for human activities attracted researchers' attention and became the focus of current research [1]. As is well-known, the amount of energy released by the sun in a few hours is far more than the energy consumed by humans all over the world throughout the year. Hence, the rational utilization of solar energy, and the decomposition of water to generate hydrogen and oxygen through sunlight, are regarded as some of the most promising ways for providing clean energy to meet the needs of sustainable development [2–4]. The decomposition of water is composed of two half reactions: the hydrogen evolution reaction (HER) and the oxygen evolution reaction (OER). The kinetic process of OER is slow and requires the participation of four electrons. This reaction process includes two important steps: O–H bond breaking and O–O bond formation, which leads to a slow reaction speed and low conversion efficiency [5–7]. Therefore, the most urgent task is to find the effective water oxidation catalysts to achieve a higher catalytic water oxidation efficiency.

In fact, some transition metal compounds with good catalytic water oxidation activity show poor catalytic stability. Nevertheless, polyoxometalates (POMs), constructed by

different transition metal–oxo clusters, not only exhibit good catalytic activity towards water oxidation, but also possess high stability, including thermal stability, pH stability, and environmental stability [8–10]. More importantly, POMs exhibit fast and reversible redox behaviors while maintaining their structural integrity. Up to now, Co- [11,12], Mn- [13,14], Cu- [15,16], and Ru- [17,18] containing POMs displayed their electrocatalytic activity for water oxidation in a solution, or after assembly into films. Based on our previous research, the Mn-containing POMs Mn4, Mn6, Mn14, and Mn16, exhibit excellent potential for photoelectrocatalytic water oxidation [19–22]. Being similar to Co and Mn, nickel (Ni), as a non-noble metal with abundant reserves and low price, is proven to have high electrocatalytic activity in the OER, which attracted widespread attention [23]. However, Ni-containing POMs (Ni-POMs)-based water oxidation catalysts are rarely reported. In 2015, Li et al. synthesized a Ni-POM, $[Ni_{25}(H_2O)_2OH)_{18}(CO_3)_2(PO_4)_6(SiW_9O_{34})_6]^{50-}$ (Ni25), and prove that Ni25 has excellent photocatalytic water oxidation activity [24], and simulated photosynthesis II (PSII) by solar energy to realize water splitting. To date, no reports were found using Ni25-POMs to investigate their electrocatalytic activity, as well as photoelectrocatalytic performance, for water oxidation in a solution or composite film. Therefore, developing the scientific and practical study of an Ni25-based composite film makes it possible to photoelectrocatalyze water oxidation.

Graphene is a single atom thick sheet composed of a single layer of sp^2 hybrid carbon atoms, and its thickness is only 0.32 nm. Since graphene was discovered, it attracted extensive attention because of its unique structure [25,26]. The honeycomb structure of reduced graphene oxide (rGO) endows it with many excellent physical and chemical properties, such as high electrical conductivity, high specific surface area, fast mobility of charge carriers at room temperature, and low production cost, which makes it an excellent acceptor/transporter. Since its discovery, rGO has been regarded as a cocatalyst in the field of photocatalysis due to its excellent carrier mobility, which can effectively promote the separation and transfer of carriers, and its high light transmittance, which does not affect the light absorption of catalysts. It is an ideal platform for photogenerated charge carriers, and an ideal carrier for immobilizing electrocatalytic water oxidation catalysts [27,28]. rGO has risen as a promising candidate for photoelectronic applications, due to its excellent optical, electronic, and physical properties [29]. Thus, in this work, we chose rGO as the carrier to fix Ni25. This aimed to enhance the photoelectrocatalytic performance for water oxidation, via the synergism of Ni25 and rGO.

Since Fujishima et al. first proposed using TiO_2 as a catalyst for photoelectrocatalytic (PEC) water oxidation in 1972 [30], PEC was regarded as a very promising and sustainable method for the conversion and utilization of solar energy. Various photoelectrocatalytic materials were extensively studied to simulate the process of photosynthesis [31,32]. In 2017, Xu's group used POM CoW_{12} with a Keggin structure to modify photoanode $BiVO_4$, which significantly improves the performance of the $BiVO_4$ photoanode and the efficiency of photoelectrocatalytic water oxidation [33]. Recently, our group fabricated Mn6 and C_3N_4 composite film, with good photoelectrocatalytic performance for water oxidation [22]. The reported results indicate that the fabrication of POMs with reversible redox properties, good electrochemical stability, and semiconductors with visible light responses is an effective method to prepare a photoelectrocatalytic water oxidation catalyst with high-efficiency.

The layer-by-layer (LBL) self-assembly method is a very useful technique to construct the composite films, due to the low operation cost, simple process, and easy control of film thickness. Its working principle is based on the electrostatic attraction between positive and negative charges. As the surface of POMs have rich negative charges, most POMs-based composite films are constructed using the LBL method, showing that the property of POMs can be maintained in the composite films, and the composite films have very good stability [34,35]. Therefore, in this work, we used the LBL method to make a composite film on the ITO electrode, by alternately adsorbing negatively charged Ni25 and positively charged PDDA or PDDA–rGO. PDDA–rGO gives rGO excellent dispersibility and positive charge [36], which can enhance the loading amount of Ni25. Furthermore,

XPS, SEM, EIS, UV–visible spectroscopy, and electrochemistry techniques were used to characterize the composite films modified electrodes. The photoelectrocatalytic performances of the composite films modified electrodes were assessed for water oxidation under light illumination.

2. Result and Discussion

2.1. Electrochemical Property of Ni25 in Solution

The electrochemical feature of Ni25 was studied in buffer solution at pH 6. Figure 1 shows the CV curves of 0.1 mM Ni25 solution at −1.2 to 0 V and 0 to 1.5 V, respectively. It is seen that in the negative potential range of −1.2 to −0.5 V, the redox peaks of W appear, whereas in the positive potential range of 1.0 to 1.4 V, the redox peak of Ni is observed, corresponding to $Ni^{2+} \rightarrow Ni^{3+}/Ni^{4+}$ at ca. 1.2 V. In addition, in the potential range of 1.3 to 1.5 V, a sharp oxidation peak indicates that the oxygen evolution process originates from the electrocatalytic water oxidation of Ni25. The same observation is described during the generation of radicals, including O*, *OH, and *OOH [23].

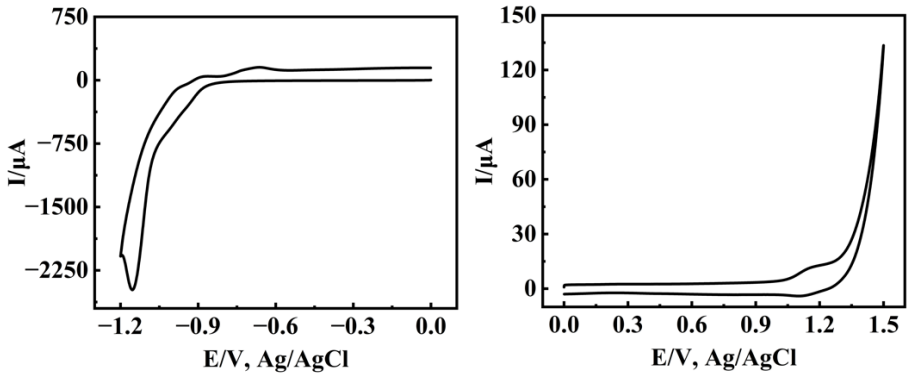

Figure 1. CVs of 0.1 mM Ni25 in 1 M NaAc + HAc (pH 6) at the scan rate of 50 mV s^{-1} using the ITO electrode.

The redox processes of Ni exhibit pH-dependent behaviors, as shown in Figure 2. Three buffer solutions of pH 4, 5, and 6 were used for testing, and it is found that the redox peak of Ni moves to the negative potential direction with the increase of pH, which indicates that protons participate in the redox process of Ni. In the acidic environment, the higher the pH, the better the electrocatalytic effect of Ni25, so the buffer solution with pH 6 was selected for subsequent experiments.

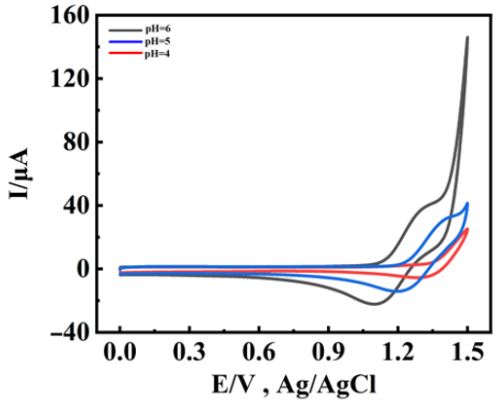

Figure 2. CVs of 0.1 mM Ni25 in 1 M NaAc + HAc with different pH values (4, red curve; 5, blue curve; and 6, black curve) at the scan rate of 50 mV s^{-1} using the ITO electrode.

Furthermore, we also studied the changes in the redox current of the Ni25 solution (0.1 mM) at different scan rates, from 40 to 200 mV s^{-1}, and the current of the Ni oxidation

peak is proportional to the square root of the scan rate (Figure S1). The results indicate that this is a diffusion-controlled process.

2.2. Characterization of the Composite Films Containing Ni25

The UV–vis spectra of the Ni25 solution, PDDA–rGO suspension, and the composite film PDDA/[Ni25/(PDDA–rGO)]$_1$ between 200–800 nm are shown in Figure 3. It is seen that the spectrum of Ni25 (red curve) exhibits an absorption peak at 252 nm, which is the feature of POMs corresponding to transition of W–O. The UV–vis spectrum of PDDA has no absorption peak between 200–800 nm, but the spectrum of PDDA–rGO (blue curve) exhibits a shoulder at 266 nm; this is the same as the characteristics of rGO in the UV–vis spectrum, which is attributed to the n-π^* transition of the C=O bond [36]. The composite film PDDA/[Ni25/(PDDA–rGO)]$_1$ (black curve) shows a characteristic absorption peak at 256 nm, which is attributed to overlap of the Ni25 and PDDA–rGO bands, indicating Ni25 and rGO are encapsulated in the composite film. Moreover, in the visible region, the component PDDA–rGO and the composite film PDDA/[Ni25/(PDDA–rGO)]$_1$ both display obvious absorption, confirming that the introduction of rGO enhances the adsorption of visible light for the composite film.

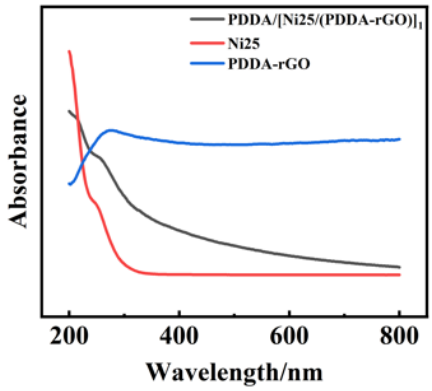

Figure 3. UV−vis spectra of Ni25 solution (red curve), PDDA−rGO suspension (blue curve) and the composite film PDDA/[Ni25/(PDDA−rGO)]$_1$ (black curve).

The UV–vis spectra of the two composite films, [PDDA/Ni25]$_n$ and PDDA/[Ni25/(PDDA–rGO)]$_n$ (n = 1~6), during the fabrication process are shown in Figures 4 and 5. It is observed that as the number of assembled layers increases, the absorbance of the characteristic peak increases linearly, which proves that these two composite films achieve uniform growth on the quartz slides.

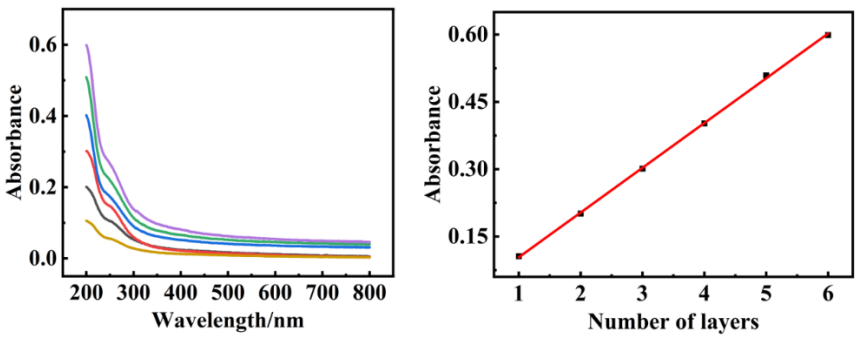

Figure 4. (**left**) UV−vis absorption spectra of the films [PDDA/Ni25]$_n$ recorded on the quartz slide with the layer numbers increasing from 1 to 6. (**right**) The relationship between the absorbance and the layer numbers at 200 nm.

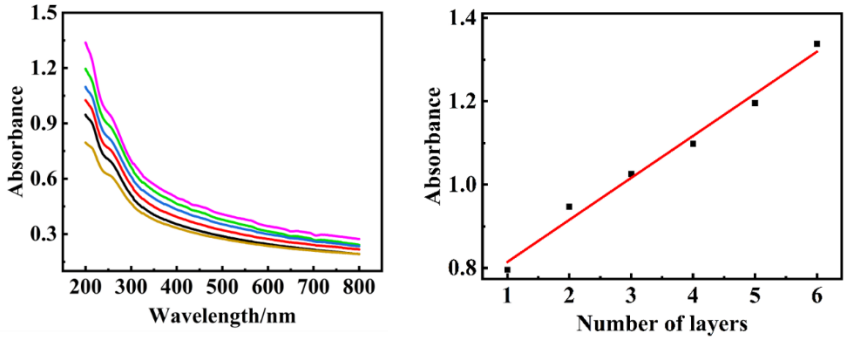

Figure 5. (**left**) UV−vis absorption spectra of the films PDDA/[Ni25/(PDDA−rGO)]$_n$ recorded on the quartz slide with the layer numbers increasing from 1 to 6. (**right**) The relationship between the absorbance and the layer numbers at 200 nm.

Moreover, the molar absorption coefficient of Ni25 in solution was calculated according to the Lambert–Beer law, A = εcL (ε is the molar absorption coefficient, c is the solution concentration, and L is the optical path). According to the characteristic absorption peak of Ni25 at 256 nm in UV–vis spectrum (Figure S2) (A = 0.686), the molar absorption coefficient of Ni25 is calculated to be ε_{Ni25} = 686,000 (mol^{-1} cm^2). The data were used to calculate the surface coverage of Ni25 on the composite films. The calculation results of surface coverage (Γ) are listed in Table S1, from which it is found that, as expected, the surface coverage (Γ) of Ni25 on the film PDDA/[Ni25/(PDDA–rGO)]$_n$ (1.03×10^{17} mol cm^{-2}) is more than that on the film [PDDA/Ni25]$_n$ (0.278×10^{17} mol cm^{-2}), proving that the presence of PDDA–rGO enhances the loading amount of Ni25 definitely.

Two composite films, [PDDA/Ni25]$_6$ and PDDA/[Ni25/(PDDA–rGO)]$_6$, were constructed on ITO, and their morphologies examined using the SEM technique. As shown in Figure S3, the SEM micrographs reveal that the Ni25 is deposited on the composite films. In addition, Figure S3b displays a typical image of graphene with a crumpled sheet, on which the species of Ni25 are uniformly dispersed. Further, the chemical composition of the two composite films were analyzed by XPS, as presented in Figure S4 for the full spectrum, confirming the presence of the elements, such as Ni, W, O, and Si for Ni25, and C, O, and N for PDDA and rGO. For clarity, Figure 6 shows the high-resolution spectra of Ni 2p and C 1s orbits, respectively. For the Ni 2p spectrum, two peaks located at 856.1 eV (Ni $2p_{3/2}$) and 873.5 eV (Ni $2p_{1/2}$) accompanied by two satellite peaks indicate the presence of Ni^{2+}. The signal peaks of C1s appear at 284.8, 286.4, and 288.1 eV, corresponding to the C–C, C–O, and O–C=O groups in the PDDA–rGO, respectively. Based on above results, it is concluded that the composite film PDDA/[Ni25/(PDDA–rGO)]$_n$ is successfully constructed.

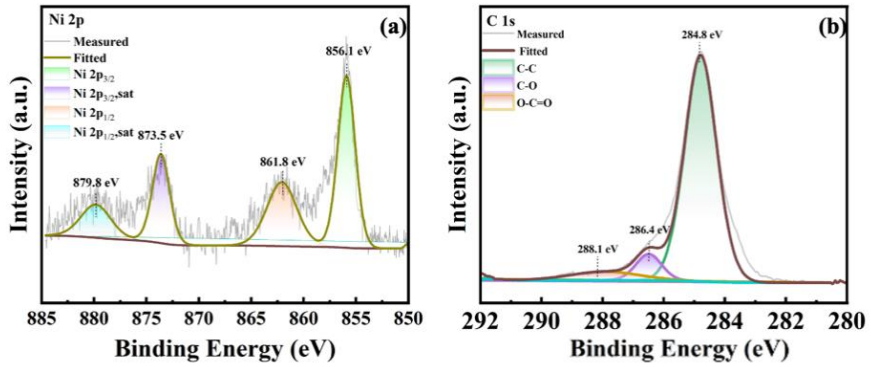

Figure 6. XPS spectra of Ni 2p (**a**) and C 1s (**b**) binding energies on the film PDDA/[Ni25/(PDDA−rGO)]$_6$/ITO.

2.3. Study on Electrocatalytic Water Oxidation for Two Composite Films

Cyclic voltammetry was further used to test the changes in the currents of water oxidation during the fabrication process of the composite films on the ITO electrode. As depicted in Figure 7, in the potential range of 0 to 1.5 V, with the number of assembled layers increased, the water oxidation currents have a good linear relationship with the layer number, proving the uniform growth of the composite film on the ITO electrode. At the same time, the CVs at 0 to 1.2 V were recorded using different scanning rates, from 50 to 500 mV s^{-1}. It is found that there is good linear relationship between the peak currents and scanning rates for the redox peaks of Ni25, suggesting a surface-confined process of Ni25 on the composite film (Figure S5), which is different from the redox behavior of Ni25 in solution, suggesting that Ni25 is successfully fabricated on the composite films.

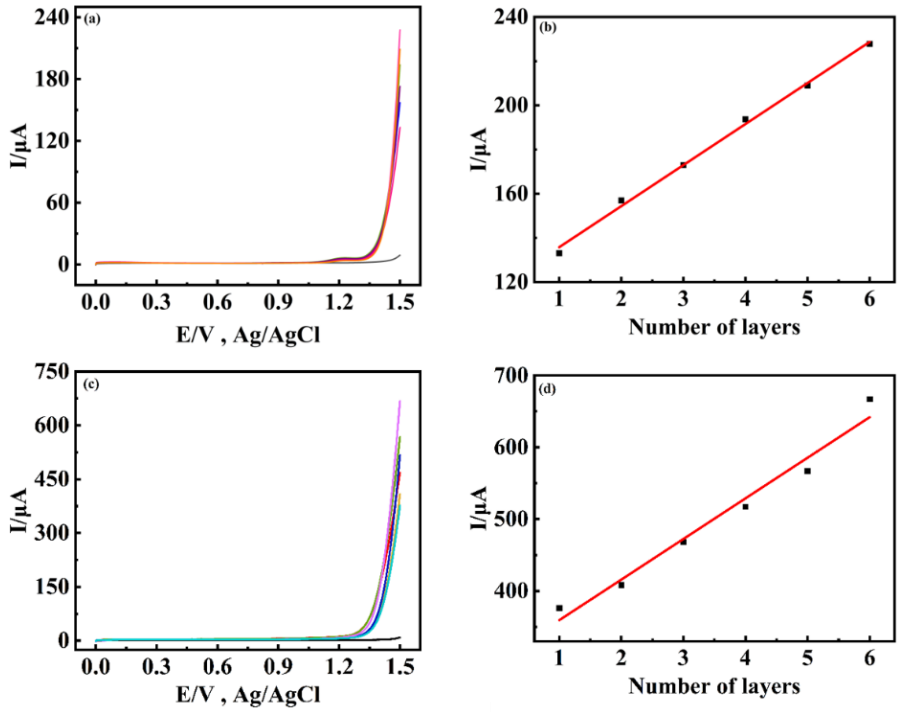

Figure 7. The electrocatalytic water oxidation curves of two composite films $[PDDA/Ni25]_n$ (n = 1−6) (**a**), and $PDDA/[Ni25/(PDDA-rGO)]_n$ (n = 1−6) (**c**), deposited on ITO in 1 M NaAc + HAc at pH 6. Scan rate: 50 mV s^{-1}. The black curve represents the electrocatalytic water oxidation curve of bare ITO electrode. The relationship between the currents and the layer numbers at 1.5 V for $[PDDA/Ni25]_n$ (**b**), and $PDDA/[Ni25/(PDDA-rGO)]_n$ (**d**).

Additionally, when compared with each other, it is observed that the composite film $PDDA/[Ni25/(PDDA–rGO)]_n$ exhibits higher catalytic currents compared to the film $[PDDA/Ni25]_n$. For instance, when the number of assembled layers of the two composite films is six, the electrocatalytic current of the film $PDDA/[Ni25/(PDDA–rGO)]_n$ is three times more than that of the film $[PDDA/Ni25]_n$. This may be attributed to the synergistic effect of rGO and Ni25, which greatly improves the electrocatalytic water oxidation performance.

2.4. Visible-Light-Driven Photoelectrocatalytic Water Oxidation

The UV–vis absorption spectrum of PDDA–rGO in aqueous solution is shown in Figure 3 (blue curve). PDDA–rGO exhibits a wide absorption peak in the UV–vis region, indicating that PDDA–rGO possesses the ability to absorb the visible light. Therefore, it is expected that the composite film $PDDA/[Ni25/(PDDA–rGO)]_n$ will show a good photoelectrocatalytic performance for water oxidation. Hence, taking an incandescent lamp as the visible light source, we investigated th photoelectrocatalytic performance of the two composite films for water oxida-

tion under dark conditions and illumination for 15 min. The results are described in Figure 8, which clearly shows that when the two composite films have the same number of assembled layers of Ni25, the film PDDA/[Ni25/(PDDA–rGO)]$_6$ exhibits a better photoelectrocatalytic performance (the current is increased by 33.7% after illumination) than the film [PDDA/Ni25]$_n$ (the current is increased by 19.7% after illumination); that is, the water oxidation current values increase about five times more after illumination for the film PDDA/[Ni25/(PDDA–rGO)]$_n$ (225 μA) than for the film [PDDA/Ni25]$_n$ (45 μA). For clarity, comparing the water oxidation currents of the two composite films under light and non-light conditions together is presented in Figure 8c, showing the obvious difference between them. Furthermore, we calculated the quotient ($I'_{\Delta p}$) of the photo-generated current ($I_{\Delta P} = I_{light} - I_{dark}$) of the sixth layer of films and the surface coverage, which is ($I'_{\Delta p} = I_{\Delta P}/\Gamma$). The data $I'_{\Delta p} = 1.62 \times 10^{-21}$ for Ni25 on [PDDA/Ni25]$_6$, and $I'_{\Delta p} = 2.18 \times 10^{-21}$ for Ni25 on PDDA/[Ni25/(PDDA–rGO)]$_6$ were obtained (see Table 1). It indicates that the photogenerated current per mole in the PDDA/[Ni25/(PDDA–rGO)]$_6$ film is more than that of the [PDDA/Ni25]$_6$ film, further confirming that the presence of rGO enhances the photoelectrocatalytic performance of Ni25.

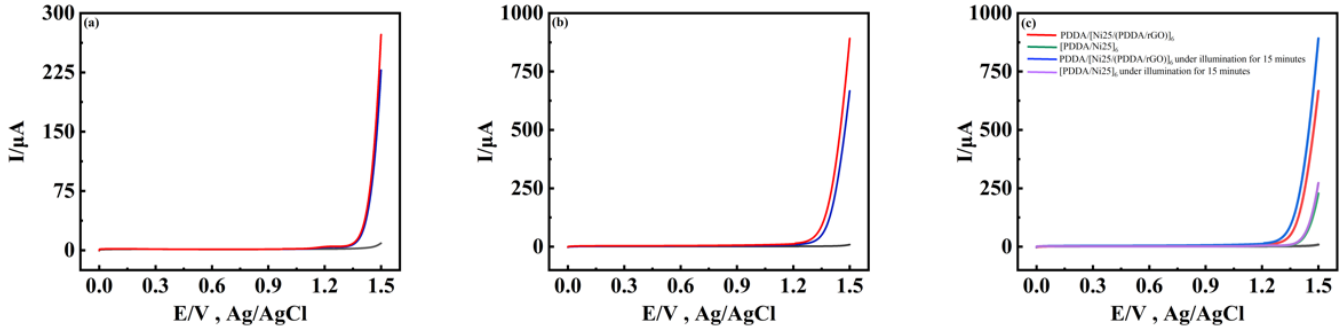

Figure 8. The comparison of the photoelectrocatalytic water oxidation of the composite films [PDDA/Ni25]$_6$ (**a**), PDDA/[Ni25/(PDDA−rGO)]$_6$ (**b**), and the combination of (**a**,**b**) (**c**). The blue curves represent the electrocatalytic water oxidation under dark conditions, red curves represent the electrocatalytic water oxidation under illumination for 15 min, the black curves represent the electrocatalytic water oxidation of bare ITO electrode, in 1 M NaAc + HAc (pH 6). Scan rate: 50 mV s^{-1}.

Table 1. *IPCE* of two films [PDDA/Ni25]$_6$ and PDDA/[Ni25/(PDDA–rGO)]$_6$.

Film	J@1.5V vs. RHE	*IPCE*
[PDDA/Ni25]$_6$	0.60 mA cm^{-2}	11.92%
PDDA/[Ni25/(PDDA–rGO)]$_6$	2.1 mA cm^{-2}	41.73%

This may be attributed to the difference in the photogenerated electron–hole recombination rate of the two composite films. In the film [PDDA/Ni25]$_n$, the photogenerated electron–hole recombination rate is fast, whereas in the film PDDA/[Ni25/(PDDA–rGO)]$_n$, the photo-induced electron and hole recombination is suppressed by rGO, leading to a lower photogenerated electron–hole recombination rate than the film [PDDA/Ni25]$_n$, which promotes the transfer of photogenerated electrons. On the other hand, the well-matched band energies and impact interaction between rGO and Ni25 highly promote the charge separation property, and shorten the migration distance of photogenerated carriers, which effectively improves the charge transfer efficiency, thereby enhancing the photoelectrocatalytic performance for water oxidation, via the synergistic effect of rGO and Ni25 [37].

In addition, in order to investigate the response of the composite films to the light, the transient photocurrent curves were recorded when the irradiation was switched on and off. As presented in Figure 9, it is clearly noted that the two composite films are sensitive to light, and both composite films show steady and reproducible photocurrent responses during several light on/off cycles using the incandescent lamp.

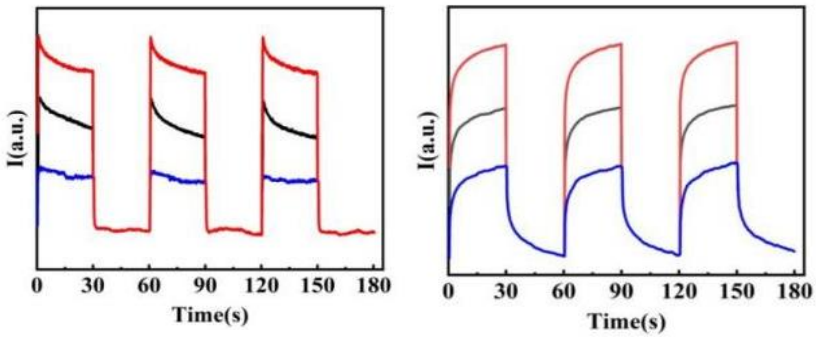

Figure 9. Transient photocurrent response of the film $[PDDA/Ni25]_n$ (n = 1, 3, 5) (**left**) and the film $PDDA/[Ni25/(PDDA-rGO)]_n$ (n = 1, 3, 5) (**right**) at 1.0 V vs. time (i−t) curve with a 30 s light on/off.

Further, it is obviously seen in Figure 9 that on the films assembled with different layers, the photogenerated currents increase as the number of layers increases regularly, and the change trend of the curves remains unchanged. This observation indicates that, on the one hand, the fabrication and performance of the two composite films have repeatability, and the two composite films are assembled uniformly, that is, the photogenerated currents versus the number of film layers have a good linear relationship, as shown in Figure S6; on the other hand, the catalytic activity can be easily controlled by the number of the layers.

Interestingly, the photocurrent curves of the two composite films show different change trends during the illumination. For the film $[PDDA/Ni25]_n$, after the illumination, the photogenerated currents rapidly rise, and then slowly decrease. This behavior can be attributed to a classical onset of recombination [38]. On the contrary, after the illumination, the photogenerated currents of the film $PDDA/[Ni25/(PDDA–rGO)]_n$ continuously increase with the extension of time, which may be caused by a trap filling [38]. The trap-induced recombination is hampered when traps are filled with the extension of time, thus, the presence of trap filling can increase the lifetime of carriers. Therefore, as the number of filled traps increases, the photocurrent gradually increases. Photoelectrocatalytic measurements show that the recombination between photo-induced holes and electrons can be suppressed by the presence of rGO. This is the reason why the photoelectrocatalytic water oxidation is more effective in the film $PDDA/[Ni25/(PDDA–rGO)]_n$ than in the film $[PDDA/Ni25]_n$.

According to the method reported in the literature [39], the effective surface areas (A_{eff}) of the two composite films were measured in 1.0 mM $[Fe(CN)_6]^{3-}/[Fe(CN)_6]^{4-}$ solution containing 0.1 M KCl, as shown in Figure S7. Based on the Randles–Savcik equation: $I_p = 2.69 \times 10^5 \times A \times n^{3/2} \times D^{1/2} \times c \times \nu^{1/2}$, I_p represents the peak current (A), A represents the effective electrode area (cm^2), n is the number of electrons transferred (n = 1), c is the concentration (mol/L), and ν is the scan rate (V/s), $D = 7.6 \times 10^{-6}$ cm^2 s^{-1}; the A_{eff} of the film $PDDA/[Ni25/(PDDA–rGO)]_4/ITO$ is 0.399 cm^2, and the A_{eff} of $[PDDA/Ni25]_4/$ ITO is 0.456 cm^2, calculated from the slope of I_p and $\nu^{1/2}$ curves. Taking the film $PDDA/[Ni25/(PDDA–rGO)]_6/ITO$ as an example, its photocurrent density reaches 2.1 mA cm^{-2} when the applied voltage is at 1.5 V vs. Ag/AgCl (see Figure 10). Compared with the water oxidation effect of the electrode $AgPW_{11}$-TiO_2/ITO, prepared by You et al. in 2018 with the photocurrent density of 1.4 mA cm^{-2} at 1.5 V vs. Ag/AgCl using a Xe lamp source (a widely used incandescent lamp with a low price) [40], the photoelectrocatalytic water oxidation efficiency of the electrode $PDDA/[Ni25/(PDDA–rGO)]_6/ITO$ reaches 1.5 times of the electrode $AgPW_{11}$-TiO_2/ITO, showing a better photocatalytic water oxidation performance. Therefore, this study indicates that the developed composite film $PDDA/[Ni25/(PDDA–rGO)]_6$ is a promising photoelectrocatalyst for water oxidation.

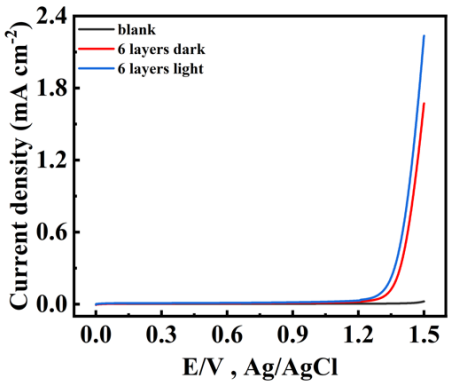

Figure 10. Current density−voltage curves of PDDA/[Ni25/(PDDA−rGO)]$_6$/ITO in the dark (red curve), and after illumination of 15 min (blue curve) in 1 M NaAc + HAc (pH 6) buffer solution. Scan rate: 50 mV/s.

The photoelectric catalytic performance of the composite films were further evaluated by the incident photocurrent conversion efficiency (*IPCE*), which is calculated by the following equation [41]:

$$IPCE = \frac{\frac{electrons}{\frac{cm^2}{s}}}{\frac{photons}{\frac{cm^2}{s}}} = \frac{J\left(\frac{mA}{cm^2}\right) \times 1240(V \times nm)}{P\left(\frac{mW}{cm^2}\right) \times \lambda}$$

where J is the photocurrent density (mA/cm^2), λ is the excitation wavelength (nm), and P is the incident light intensity (mW/cm^2). The *IPCE* of the two films, [PDDA/Ni25]$_6$ and PDDA/[Ni25/(PDDA–rGO)]$_6$, were calculated according to that the lowest wavelength (400 nm), and the intensity of incident light is 0.156 mW/cm^2. The results are listed in Table 1; it is clear that the film PDDA/[Ni25/(PDDA–rGO)]$_6$ shows higher *IPCE* than the film [PDDA/Ni25]$_6$, which confirms the enhanced photoelectrocatalytic performance of the film PDDA/[Ni25/(PDDA–rGO)]$_6$ after combining with rGO.

Electrochemical impedance spectroscopy (EIS) can reflect the transfer resistance and separation efficiency of charge carriers, thus, we measured EIS of the two films, as shown in Figure 11. It is observed that the arc radius on the Nyquist plot of the film PDDA/[Ni25/(PDDA–rGO)]$_6$ is smaller than the film [PDDA/Ni25]$_6$. This represents a lower charge-transfer resistance, which ensures the faster electron transfer. Namely, the composite film PDDA/[Ni25/(PDDA–rGO)]$_6$ can effectively inhibit the recombination of photogenerated electron–hole pairs, thereby enhancing the PEC performance.

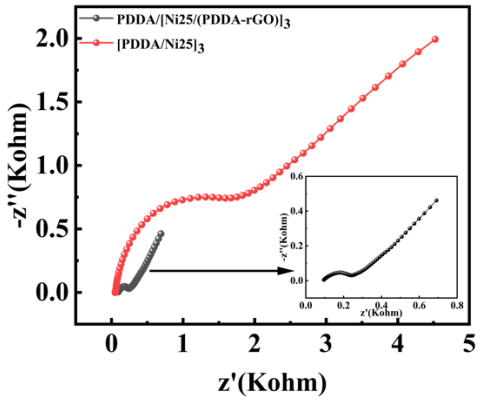

Figure 11. EIS spectra of two films [PDDA/Ni25]$_6$ and PDDA/[Ni25/(PDDA−rGO)]$_6$.

2.5. Plausible Mechanism of Photoelectrocatalytic Water Oxidation

In order to achieve efficient charge separation, and satisfy the activation energy required for this non-spontaneous reaction under solar irradiation, the lowest unoccupied molecular orbital (LUMO) and highest occupied molecular orbital (HOMO) of catalysts must be lower than 0 V and higher than +1.23 V (vs NHE, pH = 0), respectively [42]. The band gap of Ni25 is 2.23 eV, the HOMO is +1.74 V, and LUMO is −0.49 V, reported in the literature [24]. The LUMO of rGO at −0.08 V vs. NHE [43] is slightly lower than the conduction band (CB) of Ni25 (−0.49 V vs. NHE), and this indicates that rGO acts as an electron acceptor and transporter to inhibit the recombination of photo-induced electrons and holes on Ni25. The positive holes in valence band (VB) of Ni25 (+1.74 V vs. NHE) have sufficient redox potential for the oxidation of H_2O to O_2. rGO also has sufficient redox potential to reduce H^+ ions to H_2. In this process, rGO not only accelerates electron transport and inhibits charge recombination, but also improves the visible light absorption and photoelectric conversion efficiency of the film PDDA/[Ni25/(PDDA–rGO)]$_n$, facilitating the photogenerated hole oxidation reaction, and improving the PEC performance. (see Figure 12).

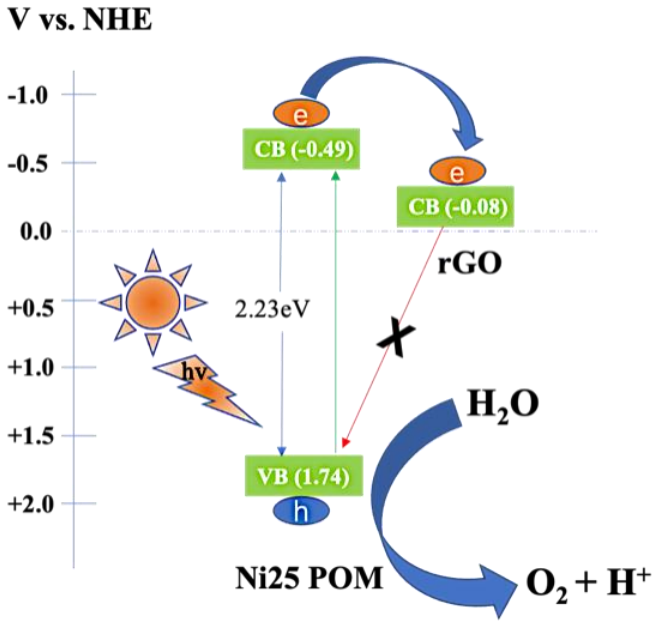

Figure 12. Plausible mechanism of photoelectrocatalytic water oxidation.

2.6. Stability Study of Ni25 in Solution and on the Composite Films

In order to check the stability of Ni25 in solution, Ni25 was dissolved in different pH buffer solutions and stored in air for 24 h, and then their UV–vis spectra were recorded. Their UV–vis spectra are shown in Figure S8, and it is seen that the absorbance of Ni25 in solution remains almost unchanged, proving the excellent stability of Ni25 in solution. Further, the stability of Ni25 in the two composite films was evaluated by electrochemistry. The two films were placed in the buffer solution (pH 6), and cyclic voltammetry was used to scan for 100 cycles, as shown in Figure S9. By calculating the percentage of current decrease before and after scanning for the two films, [PDDA/Ni25]$_6$ and PDDA/[Ni25/(PDDA–rGO)]$_6$, the oxidation current of $Ni^{2+} \rightarrow Ni^{3+}/Ni^{4+}$ decreases by 4.1% and 3.8%, respectively. The results indicate that both films have good stability, and have potential use as water oxidation photoelectrocatalysts.

3. Materials and Methods

3.1. Materials

$Na_{50}[Ni_{25}(H_2O)_2OH)_{18}(CO_3)_2(PO_4)_6(SiW_9O_{34})_6]\cdot 85H_2O$ was synthesized according to the published paper [24]. Graphene oxide was prepared according to the literature by a modified Hummers method, originally presented by Kovtyukhova and colleagues [44]. Then, it was modified in this experiment [45]. Poly(diallyldimethylammonium chloride) (PDDA Mw = 100,000–200,000, 20 wt% in water) was purchased from Aldrich. PDDA-modified reduced graphene oxide (PDDA–rGO) was synthesized according to the literature [27].

3.2. LBL Assembled Composite Film

3.2.1. Preparation of the Composite Film $[PDDA/Ni25]_n$

In the experiment, ITO electrodes or quartz plates were used as the substrates. Before the experiment, they were placed in a PDDA solution with a concentration of 8% and soaked for 2 h to form positively charged surfaces, followed by washing with deionized water and drying with N_2. The PDDA-coated substrates were then alternately and repeatedly soaked in Ni25 solution (1 mM) and PDDA solution for 20 min to obtain the composite film, which were then washed and dried. The composite film was described as $[PDDA/Ni25]_n$.

3.2.2. Preparation of the Composite Film $PDDA/[Ni25/(PDDA–rGO)]_n$

The composite film $PDDA/[Ni25/(PDDA–rGO)]_n$ was constructed using the same process as $[PDDA/Ni25]_n$. After soaking the substrate in PDDA solution (8.0 wt%) for 2 h, washing the surface with deionized water, and drying with N_2, the PDDA-coated substrate was alternately and repeatedly soaked in Ni25 solution (1 mM) and PDDA–rGO solution (1 mg mL^{-1}) for 20 min to construct the composite film, followed by washing and drying. The composite film was described as $PDDA/[Ni25/(PDDA–rGO)]_n$.

4. Conclusions

Through reasonable design, two composite films containing Ni25 were prepared by the LBL self-assembly method, $[PDDA/Ni25]_n$ (film 1) and $PDDA/[Ni25/(PDDA–rGO)]_n$ (film 2), which were characterized by XPS, SEM, and UV–vis spectra, proving their uniform assembly. The results of the electrocatalytic and photoelectrocatalytic performance towards water oxidation indicate that (1) both composite films exhibit high electrocatalytic water oxidation activity, due to the structure of the Ni–O cluster in Ni25 that is similar to the natural oxygen evolution center; (2) the photoelectrocatalytic performance of the two films increases linearly with the number of assembled layers, suggesting the uniformity and sustainability of the two films; (3) film 2 displays better catalytic activity than film 1, which is attributed to the presence of rGO in film 2. Introducing rGO to film 2 not only increases the loading amount of Ni25, but also reduces the photogenerated electron–hole recombination rate, owing to the structural feature and property of rGO. This observation is further supported by the transient photocurrent response curves, showing the case of trap filling, which greatly improves the photoelectric conversion efficiency and photocurrent response of film 2. Further, the EIS measurements demonstrate that the film $PDDA/[Ni25/(PDDA–rGO)]_n$ inhibits the recombination of photogenerated electron–hole pairs, thereby promoting the charge transfer process at the electrode/electrolyte interface. The calculation of *IPCE* confirms the positive effect of bandgap engineering on light utilization. In addition, the two films possess good stability and repeatability, confirming their research value. Compared to the light source used in the literature, we utilized a common incandescent lamp with a low price as a light source, but the developed film 2 exhibits an excellent photoelectrocatalytic performance for water oxidation, demonstrating that film 2 is a promising photoelectrocatalyst for application to the splitting of water to produce clean energy.

Supplementary Materials: The following supporting information can be downloaded at: https://www.mdpi.com/article/10.3390/catal12070696/s1, Figure S1: CVs of Ni25 in solutions at different scan rates; Figure S2: UV–vis spectrum of Ni25 in solution.; Figure S3: SEM images of two films; Figure S4: XPS spectra of two films; Figure S5: CVs of the film at different scan rates; Figure S6: The relationship of the photogenerated currents vs. the different number of layers; Figure S7: CVs of two films in $[Fe(CN)_6]^{3-}$ solution at increasing scan rates; Figure S8: UV–vis spectra of Ni25 under different conditions; Figure S9: CVs of two films with different cycles; Table S1: Comparison of the catalytic activities of Ni25 on two films.

Author Contributions: Conceptualization. J.P. and L.B.; validation, J.P. and L.B.; formal analysis, J.P. and L.B.; investigation, J.P. and L.B.; resources, J.P.; data curation, J.P.; writing—original draft preparation, J.P.; writing—review and editing, J.P. and L.B.; visualization, J.P.; supervision, L.B. All authors have read and agreed to the published version of the manuscript.

Funding: This research received no external funding.

Data Availability Statement: The data presented in this study are available on request from the corresponding author. The data are not publicly available due to the need of follow-up research.

Acknowledgments: Thanks are given to the co-authors for their help in writing this article. Thanks are given to the reviewers for their comments and valuable opinions.

Conflicts of Interest: The authors declared that they have no conflicts of interest.

References

1. Lewis, N.S. Toward Cost-Effective Solar Energy Use. *Science* **2007**, *315*, 798–801. [CrossRef]
2. Liu, G.J.; Shi, J.Y.; Zhang, F.X.; Chen, Z.; Han, J.F.; Ding, C.M.; Chen, S.S.; Wang, Z.L.; Han, H.X.; Li, C. A Tantalum Nitride Photoanode Modified with a Hole-Storage Layer for Highly Stable Solar Water Splitting. *Angew. Chem. Int. Ed.* **2014**, *53*, 7295–7299. [CrossRef]
3. Yang, L.; Nandakumar, D.K.; Miao, L.Q.; Suresh, L.; Zhang, D.W.; Xiong, T.; Vaghasiya, J.V.; Kwon, K.C.; Tan, S.C. Energy Harvesting from Atmospheric Humidity by a Hydrogel-Integrated Ferroelectric-Semiconductor System. *Joule* **2020**, *4*, 176–188. [CrossRef]
4. Tachibana, Y.; Vayssieres, L.; Durrant, J.R. Artificial photosynthesis for solar water-splitting. *Nat. Photonics* **2012**, *6*, 511–518. [CrossRef]
5. Zou, Z.; Ye, J.; Sayama, K.; Arakawa, H. Direct splitting of water under visible light irradiation with an oxide semiconductor photocatalyst. *Mater. Sustain. Energy* **2010**, *704*, 293–296. [CrossRef]
6. Kanan, M.W.; Nocera, D.G. In situ formation of an oxygen-evolving catalyst in neutral water containing phosphate and Co^{2+}. *Science* **2008**, *321*, 1072–1075. [CrossRef]
7. Kärkäs, M.D.; Verho, O.; Johnston, E.V.; Åkermark, B. Artificial Photosynthesis: Molecular Systems for Catalytic Water Oxidation. *Chem. Rev.* **2014**, *114*, 11863–12001. [CrossRef]
8. Du, D.Y.; Qin, J.S.; Li, Y.G.; Li, S.L.; Lan, Y.Q.; Wang, X.L.; Saho, K.Z.; Su, Z.M.; Wang, E.B. An unprecedented 3D 8-connected pure inorganic framework based on nanosized $([Na_{12}PO_{16}H_{24}]\subset[P_4Mo_6O_{31}H_6]_4)^{15-}$ clusters and zinc cations. *Chem. Commun.* **2011**, *47*, 2832–2834. [CrossRef]
9. Hill, C.L. Introduction: PolyoxometalatesMulticomponent Molecular Vehicles To Probe Fundamental Issues and Practical Problems. *Chem. Rev.* **1998**, *98*, 1–2. [CrossRef]
10. Thiel, J.; Ritchie, C.; Streb, C.; Long, D.-L.; Cronin, L. Heteroatom-Controlled Kinetics of Switchable Polyoxometalate Frameworks. *J. Am. Chem. Soc.* **2009**, *131*, 4180–4181. [CrossRef]
11. Stracke, J.J.; Finke, R.G. Electrocatalytic Water Oxidation Beginning with the Cobalt Polyoxometalate $[Co_4(H_2O)_2(PW_9O_{34})_2]^{10-}$: Identification of Heterogeneous CoOx as the Dominant Catalyst. *J. Am. Chem. Soc.* **2011**, *133*, 14872–14875. [CrossRef]
12. Choi, Y.; Jeon, D.; Choi, Y.; Ryu, J.; Kim, B.S. Self-Assembled Supramolecular Hybrid of Carbon Nanodots and Polyoxometalates for Visible-Light-Driven Water Oxidation. *ACS Appl. Mater. Interfaces* **2018**, *10*, 13434–13441. [CrossRef]
13. Tsuji, K.; Tomita, O.; Higashi, M.; Abe, R. Manganese-substituted polyoxometalate as an effective shuttle redox mediator in Z-scheme water splitting under visible light. *ChemSusChem* **2016**, *9*, 2201–2208. [CrossRef]
14. Xing, X.L.; Wang, M.; Liu, R.J.; Zhang, S.S.; Zhang, K.; Li, B.; Zhang, G.J. Highly efficient electrochemically driven water oxidation by graphene-supported mixed-valent Mn-16-containing polyoxometalate. *Green Energy Environ.* **2016**, *1*, 138–143. [CrossRef]
15. Yu, L.; Du, X.Q.; Ding, Y.; Chen, H.L.; Zhou, P.P. Efficient visible light-driven water oxidation catalyzed by an all-inorganic copper-containing polyoxometalate. *Chem. Commun.* **2015**, *51*, 17443–17446. [CrossRef]
16. Su, X.F.; Guan, W.; Yan, L.K.; Su, Z.M. Tricopper-polyoxometalate catalysts for water oxidation: Redox-inertness of copper center. *J. Catal.* **2020**, *381*, 402–407. [CrossRef]
17. Orlandi, M.; Argazzi, R.; Sartorel, A.; Carraro, M.; Scorrano, G.; Bonchio, M.; Scandola, F. Ruthenium polyoxometalate water splitting catalyst: Very fast hole scavenging from photogenerated oxidants. *Chem. Commun.* **2010**, *46*, 3152–3154. [CrossRef]

18. Sokolov, M.N.; Adonin, S.A.; Mainichev, D.A.; Sinkevich, P.L.; Vicent, C.; Kompankov, N.B.; Gushchin, A.L.; Nadolinny, V.A.; Fedin, V.P. New {RuNO} Polyoxometalate $[PW_{11}O_{39}Ru^{II}(NO)]^{4-}$: Synthesis and Reactivity. *Inorg. Chem.* **2013**, *52*, 9675–9682. [CrossRef]
19. Haider, A.; Ibrahim, M.; Bassil, B.S.; Carey, A.M.; Viet, A.N.; Xing, X.; Ayass, W.W.; Miñambres, J.F.; Liu, R.; Zhang, G.; et al. Mixed-Valent Mn16-Containing Heteropolyanions: Tuning of Oxidation State and Associated Physicochemical Properties. *Inorg. Chem.* **2016**, *55*, 2755–2764. [CrossRef]
20. Mitchell, S.G.; Molina, P.I.; Khanra, S.; Miras, H.N.; Prescimone, A.; Cooper, G.J.T.; Winter, R.S.; Brechin, E.K.; Long, D.-L.; Cogdell, R.J.; et al. A Mixed-Valence Manganese Cubane Trapped by Inequivalent Trilacunary Polyoxometalate Ligands. *Angew. Chem.* **2011**, *123*, 9320–9323. [CrossRef]
21. Al-Oweini, R.; Sartorel, A.; Bassil, B.S.; Natali, M.; Berardi, S.; Scandola, F.; Kortz, U.; Bonchio, M. Photocatalytic Water Oxidation by a Mixed-Valent $Mn^{III}{}_3Mn^{IV}O_3$ Manganese Oxo Core that Mimics the Natural Oxygen-Evolving Center. *Angew. Chem.* **2014**, *126*, 11364–11367. [CrossRef]
22. Wu, Y.; Yu, X.X.; Fu, Z.J.; Pei, J.Y.; Bi, L.H. Fabrication of Six Manganese Containing Polyoxometalate Modified Graphite C_3N_4 Nanosheets Catalysts Used to Catalyze Water Decomposition. *Catalysts* **2021**, *11*, 856. [CrossRef]
23. Yan, J.; Kong, L.; Ji, Y.; White, J.; Li, Y.; Zhang, J.; An, P.; Liu, S.; Lee, S.-T.; Ma, T. Single atom tungsten doped ultrathin α-$Ni(OH)_2$ for enhanced electrocatalytic water oxidation. *Nat. Commun.* **2019**, *10*, 2149. [CrossRef]
24. Han, X.B.; Li, Y.G.; Zhang, Z.M.; Tan, H.Q.; Lu, Y.; Wang, E.B. Polyoxometalate-based nickel clusters as visible light-driven water oxidation catalysts. *J. Am. Chem. Soc.* **2015**, *137*, 5486–5493. [CrossRef]
25. Yu, W.; Sisi, L.; Haiyan, Y.; Jie, L. Progress in the functional modification of graphene/graphene oxide: A review. *RSC Adv.* **2020**, *10*, 15328–15345. [CrossRef]
26. Zhang, L.; Li, S.; Zhang, Z.; Tan, L.; Pang, H.; Ma, H. Facile fabrication of reduced graphene oxide and Keggin-type polyoxometalates nanocomposite film for high performance electrocatalytic oxidation of nitrite. *J. Electroanal. Chem.* **2017**, *807*, 97–103. [CrossRef]
27. Cui, L.; Pu, T.; Liu, Y.; He, X. Layer-by-layer construction of graphene/cobalt phthalocyanine composite film on activated GCE for application as a nitrite sensor. *Electrochim. Acta* **2013**, *88*, 559–564. [CrossRef]
28. Li, X.; Yu, J.; Wageh, S.; Al-Ghamdi, A.A.; Xie, J. Graphene in Photocatalysis: A Review. *Small* **2016**, *12*, 6640–6696. [CrossRef]
29. Hadadian, M.; Correa-Baena, J.; Goharshadi, E.K.; Ummadisingu, A.; Seo, J.; Luo, J.; Gholipour, S.; Zakeeruddin, S.M.; Saliba, M.; Abate, A. Enhancing efficiency of perovskite solar cells via N-doped graphene: Crystal modification and surface passivation. *Adv. Mater.* **2016**, *28*, 8681–8686. [CrossRef]
30. Finegold, L.; Cude, J.L. Biological sciences: One and two-dimensional structure of alpha-helix and beta-sheet forms of poly(L-Alanine) shown by specific heat measurements at low temperatures (1.5–20 K). *Nature* **1972**, *238*, 38–40. [CrossRef]
31. Ye, S.; Ding, C.; Chen, R.; Fan, F.; Fu, P.; Yin, H.; Wang, X.; Wang, Z.; Du, P.; Li, C. Mimicking the Key Functions of Photosystem II in Artificial Photosynthesis for Photoelectrocatalytic Water Splitting. *J. Am. Chem. Soc.* **2018**, *140*, 3250–3256. [CrossRef] [PubMed]
32. Mohamedkhair, A.K.; Drmosh, Q.A.; Qamar, M.; Yamani, Z.H. Tuning Structural Properties of WO_3 Thin Films for Photoelectrocatalytic Water Oxidation. *Catalysts* **2021**, *11*, 381. [CrossRef]
33. Xi, L.; Jin, Z.; Sun, Z.; Liu, R.; Xu, L. Enhanced photoelectrocatalytic performance for water oxidation by polyoxometalate molecular doping in BiVO4 photoanodes. *Appl. Catal. A Gen.* **2017**, *536*, 67–74. [CrossRef]
34. Niu, P.; Hao, J. Photocatalytic degradation of methyl orange by titanium dioxide-decatungstate nanocomposite films supported on glass slides. *Colloids Surfaces A Physicochem. Eng. Asp.* **2013**, *431*, 127–132. [CrossRef]
35. Li, P.; Liu, H.; Yang, J.; Sun, D.; Chen, Y.; Zhou, Y.; Cai, C.; Lu, T. A ruthenium(III) phosphonate complex on polyallylamine functionalized carbon nanotube multilayer films: Self-assembly, direct electrochemistry, and electrocatalysis. *J. Mater. Chem. B* **2014**, *2*, 102–109. [CrossRef] [PubMed]
36. Guo, Y.; Guo, S.; Ren, J.; Zhai, Y.; Dong, S.; Wang, E. Cyclodextrin functionalized graphene nanosheets with high supramolecular recognition capability: Synthesis and host-guest inclusion for enhanced electrochemical performance (ACS Nano (2010) 4 (4001–4010)). *ACS Nano* **2010**, *4*, 5512. [CrossRef]
37. Wang, H.; Liang, Y.; Liu, L.; Hu, J.; Cui, W. Highly ordered TiO_2 nanotube arrays wrapped with g-C_3N_4 nanoparticles for efficient charge separation and increased photoelectrocatalytic degradation of phenol. *J. Hazard. Mater.* **2018**, *344*, 369–380. [CrossRef]
38. Tsuchiya, H.; Macak, J.M.; Ghicov, A.; Räder, A.S.; Taveira, L.; Schmuki, P. Characterization of electronic properties of TiO_2 nanotube films. *Corros. Sci.* **2007**, *49*, 203–210. [CrossRef]
39. Jiao, J.; Zuo, J.; Pang, H.; Tan, L.; Chen, T.; Ma, H. A dopamine electrochemical sensor based on Pd-Pt alloy nanoparticles decorated polyoxometalate and multiwalled carbon nanotubes. *J. Electroanal. Chem.* **2018**, *827*, 103–111. [CrossRef]
40. Li, J.; Wang, L.; You, W.; Liu, M.; Zhang, L.; Sang, X. Catalytic effects of $[Ag(H_2O)(H_3PW_{11}O_{39})]^{3-}$ on a TiO_2 anode for water oxidation. *Cuihua Xuebao/Chinese J. Catal.* **2018**, *39*, 534–541. [CrossRef]
41. Mohanta, D.; Barman, K.; Jasimuddin, S.; Ahmaruzzaman, M. Encapsulating band gap engineered $CoSnO_3$ mixed metal oxide nanocomposite in rGO matrix: A novel catalyst towards LED light induced photoelectrocatalytic water oxidation at neutral pH. *J. Electroanal. Chem.* **2021**, *880*, 114830. [CrossRef]
42. Zhao, C.; Chen, Z.; Shi, R.; Yang, X.; Zhang, T. Recent Advances in Conjugated Polymers for Visible-Light-Driven Water Splitting. *Adv. Mater.* **2020**, *32*, e1907296. [CrossRef] [PubMed]

43. Tran, P.D.; Batabyal, S.K.; Pramana, S.S.; Barber, J.; Wong, L.H.; Loo, S.C.J. A cuprous oxide-reduced graphene oxide (Cu_2O-rGO) composite photocatalyst for hydrogen generation: Employing rGO as an electron acceptor to enhance the photocatalytic activity and stability of Cu_2O. *Nanoscale* **2012**, *4*, 3875–3878. [CrossRef] [PubMed]
44. Hummers, W.S.; Offeman, R.E. Preparation of Graphitic Oxide. *J. Am. Chem. Soc.* **1958**, *80*, 1339. [CrossRef]
45. Kovtyukhova, N.I.; Ollivier, P.J.; Martin, B.R.; Mallouk, T.E.; Chizhik, S.A.; Buzaneva, E.V.; Gorchinskiy, A.D. Layer-by-Layer Assembly of Ultrathin Composite Films from Micron-Sized Graphite Oxide Sheets and Polycations. *Chem. Mater.* **1999**, *11*, 771–778. [CrossRef]